Water-mediated ion–ion interactions are enhanced at the water vapor–liquid interface

Vasudevan Venkateshwaran, Srivathsan Vembanur, and Shekhar Garde[1]

Howard P. Isermann Department of Chemical and Biological Engineering and Center for Biotechnology and Interdisciplinary Studies, Rensselaer Polytechnic Institute, Troy, NY 12180

Edited by Benjamin Widom, Cornell University, Ithaca, NY, and approved May 7, 2014 (received for review March 4, 2014)

There is overwhelming evidence that ions are present near the vapor–liquid interface of aqueous salt solutions. Charged groups can also be driven to interfaces by attaching them to hydrophobic moieties. Despite their importance in many self-assembly phenomena, how ion–ion interactions are affected by interfaces is not understood. We use molecular simulations to show that the effective forces between small ions change character dramatically near the water vapor–liquid interface. Specifically, the water-mediated attraction between oppositely charged ions is enhanced relative to that in bulk water. Further, the repulsion between like-charged ions is weaker than that expected from a continuum dielectric description and can even become attractive as the ions are drawn to the vapor side. We show that thermodynamics of ion association are governed by a delicate balance of ion hydration, interfacial tension, and restriction of capillary fluctuations at the interface, leading to nonintuitive phenomena, such as water-mediated like charge attraction. "Sticky" electrostatic interactions may have important consequences on biomolecular structure, assembly, and aggregation at soft liquid interfaces. We demonstrate this by studying an interfacially active model peptide that changes its structure from α-helical to a hairpin-turn–like one in response to charging of its ends.

potential of mean force | electrolytes | surface tension | inhomogeneous systems

Traditional models of an air–water interface of a salt solution present a picture in which salt ions are excluded from the interfacial region (1). However, recent simulations and experiments have shown that certain chaotropic ions, such as iodide, azide, and thiocyanate, can adsorb to the air–water interface (2–7). Even when ions are depleted from the interface, the extent of depletion is limited to a nanometer length scale (8). Charged species can also be driven to an air–water interface by covalently attaching them to hydrophobic moieties, as in ionic surfactants, or interfacially active proteins (9, 10). Thermodynamics of ion adsorption to interfaces are complex, determined by a balance of energetic and entropic contributions (7, 11, 12). The net energetic contribution can be favorable or unfavorable, depending on the differences between ion–water, ion–ion, and water–water interactions in bulk and at the interface. The entropic contribution is typically unfavorable due to the restriction of water molecules in the hydration shell of the ion and the corresponding pinning of capillary fluctuations at the interface (7, 13, 14). Solvent structure and fluctuations at the interface are also known to play an important role in ion dissociation pathways in the transport of ions across liquid–liquid interfaces (15). How these factors govern the effective ion–ion interactions near aqueous interfaces and, in turn, influence interfacial self-assembly and aggregation is, however, not understood.

We present results from extensive molecular simulations of ion hydration and ion–ion interactions near a water vapor–liquid interface. Our principal results are that solvent-mediated attraction between oppositely charged ions is enhanced near the interface relative to that in bulk. Further, the repulsion between like-charged ions is weaker than that expected from a continuum dielectric description and can even become attractive as the ions are drawn toward the vapor side. We show that the thermodynamics of ion association are governed by a delicate balance of ion hydration, interfacial tension, and restriction of capillary fluctuations at the interface, leading to nonintuitive phenomena, such as water-mediated attraction between like-charged ions. We demonstrate the consequences of "sticky" electrostatic interactions near the interface by studying the conformations of an interfacially active peptide. Our results have implications on interface-mediated self-assembly and suggest that water-mediated electrostatic interactions may play an even more important role at soft aqueous interfaces compared with that in bulk water. These results on ions along with the results of recent studies on hydrophobic interactions at aqueous interfaces (16–18) provide a framework for understanding and manipulating self-assembly of surfactants, peptides, proteins, and other macromolecules at interfaces.

Results and Discussion

Ion Pair Potentials of Mean Force in the Interfacial Environment. Fig. 1 summarizes how the effective interaction between oppositely charged ions is affected near an interface. Specifically, Fig. 1*B* shows the potential of mean force (PMF), $W(r|z)$, between a $M^+ - M^-$ ion pair in bulk water and at six different z locations, sampling the region from 1 nm into the liquid side ($z = 1$) to 1 nm on the vapor side of the interface ($z = -1$). The $W(r|z)$ profiles in Fig. 1*B* have been set to zero at $r = 1.2$ nm for reference. In bulk water, the $M^+ - M^-$ PMF shows features typical of solvent-mediated interactions (19, 20), with a contact minimum at $r = 0.39$ nm, a solvent-separated minimum at $r = 0.55$ nm, and a desolvation barrier between the two minima. $W(r|z)$ becomes negligible in magnitude for ion separations larger than 1 nm. The effective interaction, $W(r|z)$, between these small model ions, M^+ and M^-, at $z = 1$ nm is already similar to that in bulk water. However, as the ion pair is moved toward the interface, i.e., $z < 1$, $W(r|z)$ becomes highly sensitive to the location of the ion pair relative to the interface. There is a

Significance

Developing a framework for understanding self-assembly at aqueous interfaces requires the knowledge of how interfaces affect ionic and hydrophobic interactions in their vicinity. We use molecular simulations to focus on ion–ion interactions at the water vapor–liquid interface. We show that the effective forces between small ions change character dramatically near the interface, whereas oppositely charged ions attract each other more strongly than in bulk water and like-charged ions repel less strongly and can even attract each other when drawn to the vapor side of the interface. Our results suggest that water-mediated electrostatic interactions may play an even more important role in biological and colloidal assembly at soft aqueous interfaces compared with that in bulk.

Author contributions: V.V., S.V., and S.G. designed research; V.V., S.V., and S.G. performed research; V.V. and S.V. analyzed data; and V.V., S.V., and S.G. wrote the paper.

The authors declare no conflict of interest.

This article is a PNAS Direct Submission.

[1]To whom correspondence should be addressed. E-mail: gardes@rpi.edu.

This article contains supporting information online at www.pnas.org/lookup/suppl/doi:10.1073/pnas.1403294111/-/DCSupplemental.

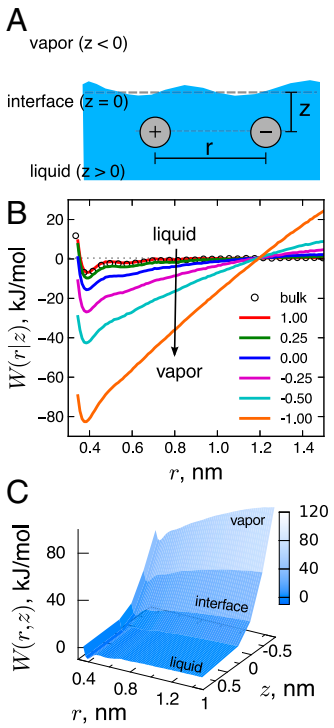

Fig. 1. (*A*) The schematic shows an oppositely charged $M^+ - M^-$ ion pair separated by r and situated in a plane at a distance z from the interface. The z axis is normal to the plane of the average vapor–liquid interface $(z = 0)$, with $z > 0$ being the liquid side. (*B*) PMF between M^+ and M^- ions calculated in various z planes. We set $W(r|z) = 0$ in each z plane at $r = 1.2$ nm for reference. (*C*) The 3D $W(r,z)$ PMF landscape for the $M^+ - M^-$ ion pair in which an ion pair separated by 1.2 nm and located at $z = 1$ is used as a reference state; i.e., $W(r = 1.2, z = 1) = 0$. This landscape highlights the work needed to move an ion pair from bulk water to the interfacial region.

monotonic decrease in the contact minimum, suggesting stronger water-mediated attraction between the $M^+ - M^-$ ion pair in the interfacial region. This is consistent with previous molecular dynamics and continuum electrostatic calculations that have shown an increased stability of a NaCl ion pair at the water–1,2-dichloroethane liquid–liquid interface (21). As the ion pair is drawn further toward the vapor side ($z \leq 0$), the effective ion–ion attraction is further strengthened, and $W(r|z)$ displays long-range correlations spanning the box length. Such long-ranged correlations are not an artifact of electrostatic calculations or the simulation methods used. By performing electrostatic calculations using the particle mesh Ewald (PME) as well as the slab Ewald summation (22), by repeating calculations for a larger box size, and by using neutral hydrophilic solutes instead of ions in independent simulations, we show later in this paper (and in *SI Text*) that these long-ranged correlations arise from capillary fluctuations and interfacial deformation.

The $W(r|z)$ profiles in Fig. 1*B* are referenced to a convenient yet arbitrary choice of $r = 1.2$ nm. We have also obtained the full 3D PMF landscape, $W(r,z)$, where only a single state on the liquid side of the interface is used as a reference; i.e., $W(r = 1.2, z = 1) = 0$ (Fig. 1*C*). This landscape highlights that work is required to move a $M^+ - M^-$ ion pair from water to the interface and to the vapor side, as reflected in the increase of $W(r,z)$ along z for most r values. Once this work is expended, the effective ion–ion attraction is stronger than that in the bulk. For certain salts this strong attraction at the interface may even drive ion pairs from bulk water to the interface (23). Such an enhancement of ion density at the interface is thought to underlie the "Ray-Jones" effect (24, 25), especially at low bulk concentrations. The enhancement of ion density near the interface coupled with ion-induced quenching of capillary waves may lead to layering of ions in the direction perpendicular to the interface. Recent X-ray reflectivity experiments have shown layering of erbium chloride at the air–water interface (26).

What are the molecular origins of enhanced ion–ion attractions at the interface? A simple dielectric description of the interface would suggest a lower dielectric constant there and, correspondingly, lower screening of ion–ion interactions compared with that in bulk water. The observed stronger attraction between the $M^+ - M^-$ ions is qualitatively consistent with such an expectation. However, for like-charged ions, the dielectric description would suggest a stronger repulsion near the vapor–liquid interface, becoming more pronounced as the ions are drawn to the vapor side. Such enhanced repulsion is not observed in our simulations. Fig. 2 shows the $W(r|z)$ profiles for like-charged $M^+ - M^+$ and $M^- - M^-$ ion pairs at various z locations. In bulk water, as expected, the direct ion–ion electrostatic repulsion dominates the short-range part ($r < 0.5$ nm). At intermediate separations, $0.5 < r < 1$ nm, $W(r|z)$ profiles for both ion pairs show small oscillations, reflecting the effects of solvent structuring in ion hydration shells. The first minimum in $W(r|z)$ profiles at $r \approx 0.55$ nm is not a "contact minimum" but corresponds to a "water-bridged" configuration, in which a few hydration water molecules shared by both ions mediate their interaction. Structural details of such solvent-bridged minimum configurations have been reported previously for like-charged halide ion pairs (27, 28). PMFs for both ion pairs become negligible for $r > 1$ nm in bulk water.

In contrast to the expectations of continuum dielectric models, the like-charged ion–ion PMFs display an overall strengthening of their effective attraction near the interface and especially on the vapor side. The stronger preference for water-bridged configurations is reflected in the deep minimum at $r \approx 0.55$ nm, in the $M^- - M^-$ PMF at $z = -1$. Interestingly, some oscillations in the PMF are retained even at $z = -1$, suggesting that ions are partially hydrated on the vapor side of the interface.

Ion Solvation Thermodynamics. To understand the above counterintuitive results, we first focus on single-ion solvation near the interface. We define $\Delta G(z)$ as the free energy or the reversible work required to move a solute from the liquid side of the interface $(z = 1)$ to a given z location. Fig. 3 shows $\Delta G(z)$ for

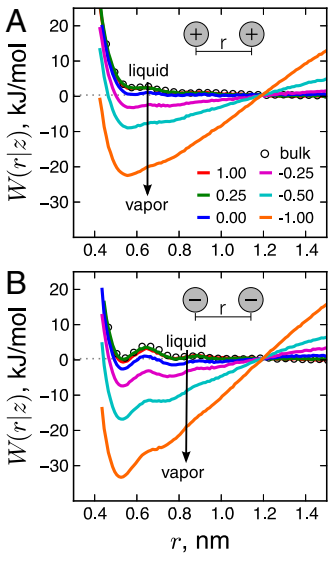

Fig. 2. (*A* and *B*) PMFs between like charges (*A*) $M^+ - M^+$ and (*B*) $M^- - M^-$ at various z locations in the interfacial region. For reference, we set the PMF profile in each z plane to zero at $r = 1.2$ nm. The effective repulsion between like-charged ions is not enhanced. In fact, ion–ion interactions can become attractive on the vapor side as indicated by PMFs for $z < 0$.

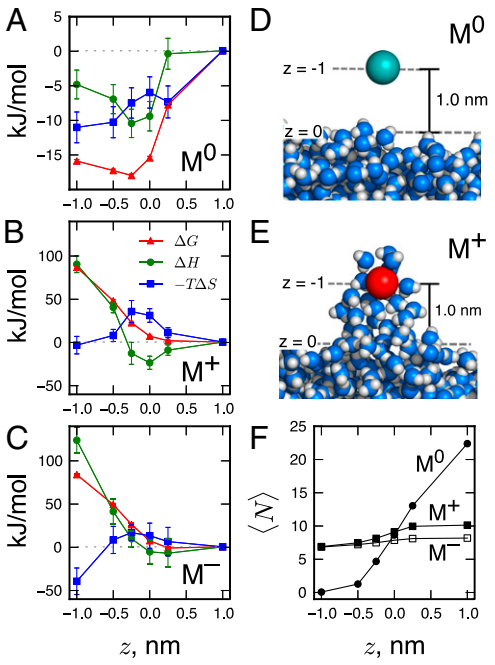

Fig. 3. (*A–C*) Free energy (ΔG), enthalpy (ΔH), and entropy ($-T\Delta S$) of moving a solute from bulk water to a given z location for (*A*) M^0 solute and (*B*) M^+ and (*C*) M^- ions. (*D* and *E*) Simulation snapshots show that the M^0 solute is fully dehydrated (*D*), whereas the M^+ ion remains partially hydrated (*E*), deforming the interface when pulled to $z=-1$. (*F*) The average number, $\langle N\rangle$, of water oxygen centers in the first hydration shell of the ions and of the neutral solute at various z locations. The hydration shell radius is defined by the first minimum in the solute–water radial distribution function in bulk water.

M^+ and M^- ions and a neutral M^0 solute. Water-to-vapor transfer of the neutral/hydrophobic (i.e., M^0) solute is favorable, and its thermodynamics are well understood (16, 29–32). Indeed, $\Delta G(z)$ at $z=-1$ is negative and is favored by a positive entropy change, and its value matches the water-to-vapor transfer free energy calculated using Widom's insertion method (33). This is expected as the M^0 solute is completely dehydrated at $z=-1$ (Fig. 3 *D* and *F*). The $\Delta G(z)$ profile displays a minimum slightly to the vapor side of the interface, reflecting favorable energetic interactions of the M^0 solute with the aqueous phase (3, 32).

In contrast, $\Delta G(z)$ values for both M^+ and M^- ions increase monotonically to small positive values as the ions are moved from liquid to the interface. As the ions are drawn further into the vapor phase, $\Delta G(z)$ increases dramatically, reaching $\approx +90$ kJ/mol for both M^+ and M^- ions at $z=-1$. Details of the $\Delta G(z)$ profile depend on the size and the charge density of the ions. Even though there is no minimum in $\Delta G(z)$ profiles at the interface for M^+ and M^- ions studied here, a minimum does exist for ions having lower charge densities as shown by Otten et al. (7).

Despite the large amount of work required to pull the ions away from the liquid phase, as reflected in the large positive $\Delta G(z)$ at $z=-1$, its magnitude is only 20–25% of the liquid-to-vacuum transfer free energy of these ions ($\approx +380$ kJ/mol for the M^+ ion and $\approx +450$ kJ/mol for the M^- ion). This observation suggests that the ions are not completely dehydrated at $z=-1$. Indeed, Fig. 3 *E* and *F* shows that the ions are able to maintain most of their hydration water molecules by deforming the vapor–liquid interface. The M^- and M^+ ions lose only about 2 and 4 molecules, of 8 and 10 hydration shell water molecules in the bulk, respectively. That the M^- ion retains a larger fraction of its hydration water is consistent with the more favorable hydration of negative ions compared with positive ions of the same size (34–37). Interfacial deformation following the movement of ions across soft aqueous interfaces has been observed in previous simulation studies (3, 38).

Both interface deformation and partial dehydration of ions contribute to $\Delta G(z)$ for $z<0$. Below we estimate these contributions, using macroscopic interfacial thermodynamics and bulk coordination statistics to illustrate consistency with the physical picture presented above. Pulling an ion to a given z location on the vapor side increases the interfacial area by $\Delta A(z)$, and the corresponding free energy change is given by $\Delta G_{\rm def}(z)\approx\gamma\Delta A(z)$, where γ is the water vapor–liquid surface tension. We calculate $A(z)$ by applying the coarse-graining procedure of Willard and Chandler (39) to instantaneous configurations and estimate $\Delta A(z)$ as $\Delta A(z)=\langle A(z)\rangle-\langle A(z=1)\rangle$, where $\langle\rangle$ represents an ensemble average with the ion fixed at a given z location. Table 1 shows that for $-0.5<z<0$, the interface is slightly deformed, and $\Delta G_{\rm def}(z)$ accounts for ~50–60% of the overall free energy change, $\Delta G(z)$, for both the M^+ and M^- ions. As the ions are pulled further into the vapor phase, the dominant role of interface deformation becomes clear, with $\Delta G_{\rm def}(z)$ contributing as much as 70–80% of $\Delta G(z)$.

The contribution to $\Delta G(z)$ from partial dehydration of ions can be estimated from the knowledge of bulk coordination statistics of ions (40). If $P(N_{\rm sh})$ is the probability of observing $N_{\rm sh}$ water molecules in an ion's hydration shell, then the reversible work required to remove δN water molecules from the shell is given approximately by $-k_{\rm B}T\ln[P(N^*_{\rm sh}-\delta N)/P_{\rm bulk}(N^*_{\rm sh})]$, where $N^*_{\rm sh}$ is the most probable number of hydration water molecules. At $z=-1$, $\delta N=2$ and 4 for M^- and M^+ ions, respectively. For these δN values, using $P(N_{\rm sh})$ for ions in bulk water, we estimate the contribution to $\Delta G(z)$ from partial dehydration to be ~10 kJ/mol for both ions. Together, our estimates of contributions from interface deformation and partial dehydration account for ~90% of $\Delta G(z)$ at $z=-1$.

Resolving $\Delta G(z)$ into entropy and enthalpy provides further insights into the interplay of different factors—ion–water vs. water–water interactions, water structure, capillary pinning, and interface deformation—in governing the ion solvation thermodynamics near the interface (Fig. 3). The entropy contribution ($-T\Delta S$) for moving the ions from bulk water ($z=1$) to the interface ($z=0$) is unfavorable (positive) for both M^+ and M^- ions. Otten et al. showed that this unfavorable entropy arises from pinning of the capillary fluctuations by ions at the interface (7). In contrast, the enthalpy contribution (ΔH) is favorable (negative) and displays a minimum near the interface, resulting from the balance of ion–water and water–water interactions in bulk and at the interface (7). As the ions are moved from $z=0$ to $z=-1$, ΔH increases sharply by more than 100 kJ/mol, and $-T\Delta S$ decreases by ~40–50 kJ/mol. Not only the signs of changes in ΔH (unfavorable) and $-T\Delta S$ (favorable) but also their relative magnitudes are consistent with estimates from the temperature dependence of water vapor–liquid surface tension (17, 41). Creating interfacial area is enthalpically unfavorable and entropically favorable, with enthalpy dominating entropy by a factor of approximately 2. Our results together with those of Otten et al. (7) suggest that a favorable minimum in ΔH and an

Table 1. Contributions of interface deformation to single-ion solvation

Ion	Z (nm)	$\Delta A(z)$, nm^2	$\Delta G_{\rm def}(z)$, kJ/mol	$\Delta G(z)$, kJ/mol
M^+	−0.25	0.26	11.0	22.2
	−0.50	0.54	23.2	47.6
	−1.00	1.35	57.9	86.4
M^-	−0.25	0.33	14.3	25.8
	−0.50	0.70	29.8	48.9
	−1.00	1.62	69.4	83.5

An ion placed at z (for $z<0$) deforms the interface. The average increase in the area, $\Delta A(z)$, the corresponding free energy of interface deformation, $\Delta G_{\rm def}(z)$, and the overall free energy of moving an ion from bulk water to a given location z, $\Delta G(z)$, are shown. Surface tension of the SPC/E model was taken from Alejandre et al. (41).

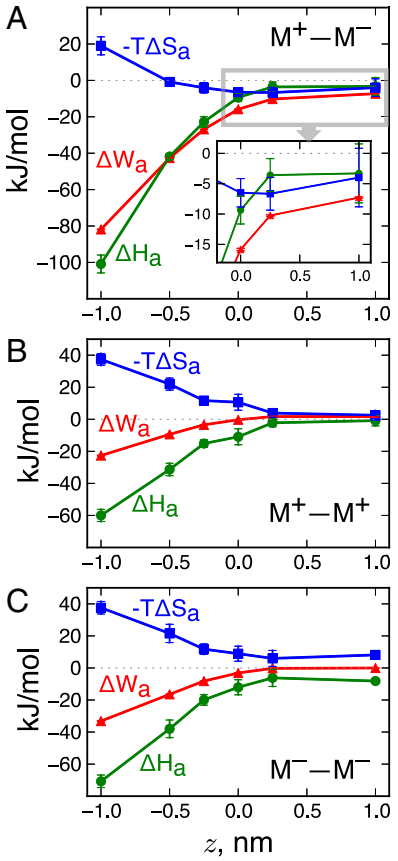

Fig. 4. (*A*–*C*) Enthalpy (ΔH_a) and entropy ($-T\Delta S_a$) contributions to the free energy of association (ΔW_a, as defined by Eq. 1) for (*A*) $M^+ - M^-$, (*B*) $M^+ - M^+$, and (*C*) $M^- - M^-$ ion pairs at various z locations. *Inset* in *A* focuses on the z locations that are on the liquid side of the interface.

unfavorable maximum in $-T\Delta S$ may be general features of ion solvation at aqueous interfaces. Whether $\Delta G(z)$ displays a minimum or not depends on their relative magnitudes, which in turn are influenced by ion size and charge density.

Thermodynamics of Ion–Ion Interactions. The $W(r|z)$ profiles in Figs. 1 and 2 characterize the distance-dependent interaction between the ions in a given z plane. For simplicity, we define $\Delta W_a(z)$ as a measure of their association strength in that plane,

$$\Delta W_a(z) = W(r_a|z) - W(r_d|z), \qquad [1]$$

where r_a and r_d are the ion–ion separations in the associated and dissociated states, respectively, with more negative values of $\Delta W_a(z)$ indicating stronger association. We use $r_d = 1.2$ nm for all of the ion pairs. For the $M^+ - M^-$ pair, we use $r_a = 0.39$ nm, corresponding to the contact minimum in the PMF. For the like-charged pairs, we use the solvent-bridged minimum as the associated state, with $r_a = 0.55$ nm for $M^+ - M^+$ and $r_a = 0.53$ nm for $M^- - M^-$ pairs, respectively.

Fig. 4*A* shows that the $M^+ - M^-$ ion pair association is favorable in water [$\Delta W_a(z) < 0$ at $z = 1$]. Both enthalpy ($\Delta H_a(z)$) and entropy ($-T\Delta S_a(z)$) contributions to $\Delta W_a(z)$ are negative (favorable) and have been shown to arise from direct ion–ion interactions and the release of restricted hydration shell water molecules upon association, respectively (42, 43). In contrast, the strength of association of like-charged ions into a solvent-bridged state is small ($\Delta W_a(z) \sim 0$) in bulk water, resulting from an approximate enthalpy–entropy compensation. This is consistent with the results of Zangi, who showed that for halide ion pairs, the enthalpy of solvent-bridged configurations is favorable and entropy is unfavorable (27). For ions with higher charge densities, the favorable enthalpic contribution can dominate, making the solvent-bridged state of the like-charged ions the most favorable configuration (27).

Ion association at the interface is more favorable than in the bulk for all ion pairs as indicated by more negative values of $\Delta W_a(z = 0)$. Fig. 4 shows that $\Delta H_a(z)$ and $-T\Delta S_a(z)$ values are correspondingly amplified at the interface. The molecular details underlying this amplification are likely subtly different for the like- and unlike-charged ion pairs. For example, the association of a $M^+ - M^-$ ion pair into the contact state is entropically favorable (Fig. 4*A*, *Inset*), consistent with the release of entropically restricted hydration water and reduced capillary pinning in the associated state. Whereas the association of $M^+ - M^+$ and $M^- - M^-$ pairs into solvent-bridged configurations remains entropically unfavorable (Fig. 4 *B* and *C*). Nevertheless, bulk-like trends with amplification are consistent with the well-hydrated state of ions at the interface.

All ion pairs display a strong tendency to associate on the vapor side. This association is dominated by interface deformation as reflected in the resolution of $\Delta W_a(z)$ into $\Delta H_a(z)$ and $-T\Delta S_a(z)$. Two separated ions deform the interface and create a larger interfacial area than does an associated pair. The decrease in interfacial area upon association is favored by enthalpy and opposed by entropy. Further, as shown for single-ion solvation in this region, the relative contributions of enthalpy and entropy are similar to those obtained from the temperature dependence of surface tension of water.

The Generality of the Mechanism Underlying Interface-Mediated Attraction Between Solutes on the Vapor Side. That interface deformation governs the effective interactions on the vapor side of the interface is not unique to ions, but is observed for solutes having strong attractive interactions with water. We illustrate this by calculating the PMF between two neutral M^0-like solutes, having ~10 times the attraction with water compared with the M^0 solute ($\sigma_{solute-water} = 0.38$ nm and $\epsilon_{solute-water} = 7.434$ kJ/mol). To eliminate contributions from direct solute–solute attraction to the PMF, our test solutes interact with each other through the purely repulsive Weeks–Chandler–Andersen potential (44).

The $W(r|z)$ profile for these solutes in bulk water shows oscillations with a well-defined solvent-separated minimum stabilized by the highly favorable solute–water interactions at $r \approx 0.80$ nm and a direct contact feature but not a contact minimum at $r \approx 0.45$ nm (Fig. 5*A*). The effective solute–solute attraction becomes stronger near the interface. At $z = -1$, the interface-mediated sticky solute–solute interaction is characterized by a broad ~60-kJ/mol deep minimum, even though there is no direct solute–solute attraction. The interface-dominated association is further evident in the $W(r|z)$ profiles at the vapor–liquid interface of an ethanol–water solution (Fig. 5*B*). Ethanol molecules are interfacially active, decrease the surface tension of water from

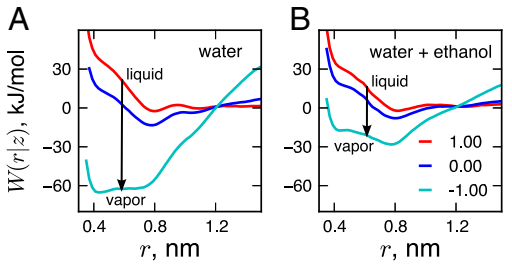

Fig. 5. (*A* and *B*) The PMFs between two M^0-like neutral solutes in (*A*) water and (*B*) 40% by mass ethanol solution at various z locations highlight the generality of the interface-dominated solute association on the vapor side of the interface. The solutes have strong attractive Lennard–Jones interactions with solvent molecules, but have repulsive Weeks–Chandler–Andersen (44) interactions with each other.

72 mN/m to 31 mN/m (45), and correspondingly reduce the driving force for solute association.

Implications for Peptides. Many biomolecules and polyelectrolytes contain ionizable groups on their surfaces and are interfacially active (46). Naturally, these molecules will carry with them their ionizable groups to the interface. Our principal result—that solvent-mediated attraction between ions is enhanced and is sensitive to their location relative to the interface—has implications on biomolecular structure and function. To demonstrate this in a model system, we performed simulations of two versions of a Gly–$(Leu)_5$–Gly peptide—an end-neutral version, $^0GL_5G^0$, where the N and C termini are capped with CH_3CO^- and $CH_3NH_2^+$ groups, respectively, and an end-charged version, $^+GL_5G^-$, where the termini are free amino (positive) and carboxyl (negative) groups, respectively. The AMBER-99SB (47) force field was used to represent the peptide. Fig. 6 shows snapshots from simulations of both peptides relative to the instantaneous aqueous interface. The hydrophobic leucine groups prefer to point to the vapor phase and make both the peptides interfacially active. The charged groups of the $^+GL_5G^-$ peptide are present in the subsurface layer, thus pulling the peptide slightly to the liquid side of the interface.

We performed 20-ns–long simulations of both peptides in bulk water and at the vapor–liquid interface and analyzed their structures, using a greedy clustering algorithm (48). To quantify the effects of charging the ends of the peptide, we calculated the PMF along the C_α–C_α end-to-end distance (r_{1-7}), using umbrella sampling simulations. The end-neutral version, $^0GL_5G^0$, folds into helical conformations at the interface, with average end-to-end distance of roughly 0.85 nm (Fig. 6*A*), at which the PMF also shows a clear minimum (Fig. 6*B*). Fig. 6 highlights the dramatic effect of charging the peptide ends. The ends of $^+GL_5G^-$ peptide form a stable contact, with the hydrophobic leucine groups pointing toward the vapor phase, leading to a hairpin-turn–like structure at the interface. Correspondingly, the end-to-end PMF shows a deep minimum at ∼0.5 nm, as expected from the enhancement of effective ion–ion attraction in the vicinity of the interface shown in Fig. 1. An alternative perspective, focused on the effect of bringing the end-charged $^+GL_5G^-$ peptide from bulk water to the interface is presented in the *SI Text*. The stronger water-mediated attraction between the oppositely charged ends of the peptide near the interface is clear in the differences between bulk and interfacial PMFs.

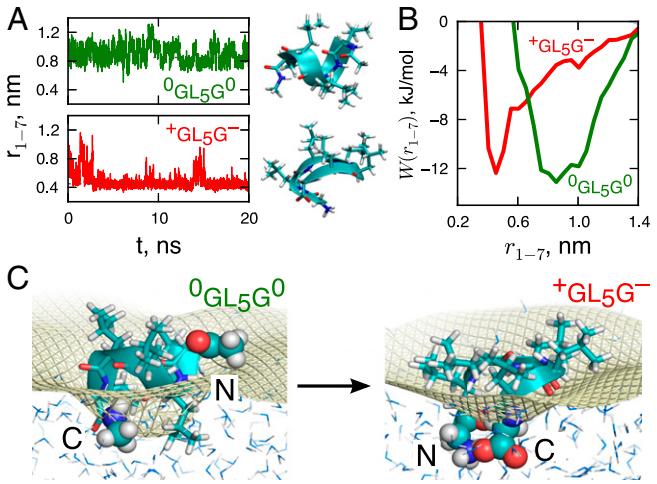

Fig. 6. The effect of charging the peptide ends on its structure at the interface. (*A*) Time dependence of the peptide C_α–C_α end-to-end distance, r_{1-7}, over a 20-ns simulation trajectory for the end-neutral and end-charged versions. The representative interfacial conformations of $^0GL_5G^0$ (α-helical) and $^+GL_5G^-$ peptides (hairpin turn) obtained using a greedy clustering algorithm (48) are also shown. (*B*) The PMF along the peptide C_α–C_α end-to-end distance calculated using umbrella sampling simulations. (*C*) Simulation snapshots of the two versions of the peptide at the water vapor–liquid interface. The peptide backbone (cartoon), the leucine groups (sticks), C and N termini of the peptide (spacefill), and water molecules (oxygen, blue; hydrogen, gray) are shown. The Willard–Chandler instantaneous interface (39) is marked by a yellow mesh.

Concluding Remarks

How water mediates interactions between ions has been reasonably well understood in bulk water (19, 20, 27, 49). We used molecular simulations to study water-mediated interactions between ions near a vapor–liquid interface of water. Our work highlights the role of different factors—water structure, capillary fluctuations, and interface deformation—that influence the effective ion–ion interactions near the interface. As an ion pair is drawn from bulk water to and across the vapor–liquid interface, the effective attraction between oppositely charged ions is significantly enhanced. Surprisingly, the repulsion between like-charged ions is not correspondingly enhanced, as would be expected from continuum dielectric treatments. In contrast, when they are drawn to the vapor side of the interface, we showed that like-charged ions can attract each other. Resolving the free energy of association into enthalpy and entropy confirms the dominant role of interface deformation in sticky water-mediated solute–solute interactions near the interface. This observation adds to the rich landscape of phenomena involving interface-dominated interactions between objects from nanoscale to millimeter and larger scales (50–52).

Interface deformation is also relevant in various processes, such as in ion transfer across soft liquid interfaces, in phase transfer catalysis (15), and in the transfer of charged peptides across lipid bilayers (53). Although such deformation may be rare in practical situations, even in the subsurface layer, the effective ion–ion attractions are sufficiently strong to affect the structure and stability of biomolecules. Indeed, our simulations of a model peptide show dramatic effects on its structure at the interface upon charging of its ends. Whereas the end-neutral peptide forms an α-helical structure, charging the ends disrupts the helix and leads to the formation of a hairpin turn stabilized by stronger charge–charge interactions. How charged species interact with each other in the interfacial environment is also relevant in many chemical and biological contexts such as emulsification (54), surfactant phase behavior (10, 55), and assembly of peptides and proteins leading to fibril formation (56, 57), to name a few. These observations combined with the recent results on how interfaces affect the strength of hydrophobic interactions (17, 18) form key elements of a framework for understanding and manipulating self-assembly at interfaces.

Materials and Methods

System. Our simulation system comprises a 4-nm-thick slab of water in contact with a 5-nm-thick vapor layer above it in the z direction, forming a vapor–liquid interface. The cross section of the simulation box is 3.5 nm × 3.46 nm in the x and y directions. The bottom layer of the water slab is anchored to a self-assembled monolayer presenting –OH head groups (58). We represent ions as spherical Lennard–Jones particles ($\sigma = 0.44$ nm, $\varepsilon = 0.85$ kJ/mol) with a charge of $q = \pm 1.2e$ placed at the ion center. For this choice of charge and ion size, the overall charge density is comparable to that of a chloride ion. We refer to the positively and negatively charged ions as M^+ and M^-, respectively. Water molecules are represented explicitly, using the extended simple point charge (SPC/E) model (59).

Simulation Details. Simulations were performed in the canonical ensemble (NVT), using the molecular dynamics package GROMACS (60). The Leapfrog algorithm with a time step of 2 fs was used to integrate the equations of motion with bond constraints on water molecules imposed using the LINCS algorithm (61). The temperature was maintained using Bussi's stochastic velocity rescaling thermostat (62). All enthalpies and entropies were obtained using simulation data at four different temperatures (287 K, 300 K, 312 K, and 325 K). Electrostatic interactions were calculated using the PME algorithm (63) with a grid spacing of 0.12 nm and a real-space cutoff of 1.3 nm. Lennard–Jones interactions were truncated at 1.3 nm. Parameters for cross-interactions were calculated using the Lorentz–Berthelot mixing rules. Configurations were stored every 0.5 ps for analysis. Ion solvation free energies were calculated using a combination of Widom's insertion (33) and free energy perturbation methods (64).

Umbrella Sampling. The ion–ion PMF profile at a given z location was calculated using the umbrella sampling method with the ion pair placed in that z plane, with the ion–ion axis parallel to the x direction. The ions were allowed to move only in that direction during the course of a given simulation. The short-range part of the PMF was sampled using four closely spaced windows corresponding to ion–ion separation, r, of 0.35 nm, 0.4 nm, 0.5 nm, and 0.6 nm. For $r = 0.6$–1.6 nm, we used five equally spaced windows to construct the longer-range part of the PMF. A harmonic umbrella potential of $0.5K(r - r_0)^2$ with $K = 500$ kJ·mol^{-1}·nm^{-2} was used in all windows. Each window was equilibrated for 1 ns, followed by 10 ns of production run. The PMF was calculated using the WHAM method (65).

ACKNOWLEDGMENTS. We thank Richard Saykally, Mark Schlossman, Phillip Geissler, Douglas Tobias, Gerhard Hummer, and Patrick Varilly for reading this manuscript and providing useful comments. We thank Center for Computational Innovations at Rensselaer Polytechnic Institute for high-performance computing resources. This work was supported by National Science Foundation Grant CBET-1159990.

1. Onsager L, Samaras NNT (1934) The surface tension of Debye-Hückel electrolytes. *J Chem Phys* 2:528–536.
2. Jungwirth P, Tobias DJ (2002) Ions at the air/water interface. *J Phys Chem B* 106(25): 6361–6373.
3. Dang LX (2002) Computational study of ion binding to the liquid interface of water. *J Phys Chem B* 106(40):10388–10394.
4. Petersen PB, Saykally RJ (2006) On the nature of ions at the liquid water surface. *Annu Rev Phys Chem* 57:333–364.
5. Jungwirth P, Tobias DJ (2006) Specific ion effects at the air/water interface. *Chem Rev* 106(4):1259–1281.
6. Netz RR, Horinek D (2012) Progress in modeling of ion effects at the vapor/water interface. *Annu Rev Phys Chem* 63:401–418.
7. Otten DE, Shaffer PR, Geissler PL, Saykally RJ (2012) Elucidating the mechanism of selective ion adsorption to the liquid water surface. *Proc Natl Acad Sci USA* 109(3):701–705.
8. Luo G, et al. (2006) Ion distributions near a liquid-liquid interface. *Science* 311(5758): 216–218.
9. Monteux C, Williams CE, Meunier J, Anthony O, Bergeron V (2004) Adsorption of oppositely charged polyelectrolyte/surfactant complexes at the air/water interface: Formation of interfacial gels. *Langmuir* 20(1):57–63.
10. Scatena LF, Richmond GL (2004) Aqueous solvation of charge at hydrophobic liquid surfaces. *Chem Phys Lett* 383(5):491–495.
11. Caleman C, Hub JS, van Maaren PJ, van der Spoel D (2011) Atomistic simulation of ion solvation in water explains surface preference of halides. *Proc Natl Acad Sci USA* 108(17):6838–6842.
12. Stern AC, Baer MD, Mundy CJ, Tobias DJ (2013) Thermodynamics of iodide adsorption at the instantaneous air-water interface. *J Chem Phys* 138(11):114709.
13. Vaikuntanathan S, Shaffer PR, Geissler PL (2013) Adsorption of solutes at liquid-vapor interfaces: Insights from lattice gas models. *Faraday Discuss* 160:63–74, discussion 103–120.
14. Ou S, Patel S (2013) Temperature dependence and energetics of single ions at the aqueous liquid-vapor interface. *J Phys Chem B* 117(21):6512–6523.
15. Benjamin I (2013) Recombination, dissociation, and transport of ion pairs across the liquid/liquid interface. Implications for phase transfer catalysis. *J Phys Chem B* 117(16):4325–4331.
16. Chandler D (2005) Interfaces and the driving force of hydrophobic assembly. *Nature* 437(7059):640–647.
17. Patel AJ, et al. (2011) Extended surfaces modulate hydrophobic interactions of neighboring solutes. *Proc Natl Acad Sci USA* 108(43):17678–17683.
18. Vembanur S, Patel AJ, Sarupria S, Garde S (2013) On the thermodynamics and kinetics of hydrophobic interactions at interfaces. *J Phys Chem B* 117(35):10261–10270.
19. Pettitt BM, Rossky PJ (1986) Alkali halides in water: Ion–solvent correlations and ion–ion potentials of mean force at infinite dilution. *J Chem Phys* 84:5836–5844.
20. Fennell CJ, Bizjak A, Vlachy V, Dill KA (2009) Ion pairing in molecular simulations of aqueous alkali halide solutions. *J Phys Chem B* 113(19):6782–6791.
21. Schweighofer K, Benjamin I (2000) Ion pairing and dissociation at liquid/liquid interfaces: Molecular dynamics and continuum models. *J Chem Phys* 112(3):1474–1482.
22. Yeh IC, Berkowitz ML (1999) Ewald summation for systems with slab geometry. *J Chem Phys* 111:3155–3162.
23. Otten D, Onorato R, Michaels R, Goodknight J, Saykally R (2012) Strong surface adsorption of aqueous sodium nitrite as an ion pair. *Chem Phys Lett* 519:45–48.
24. Jones G, Ray WA (1937) The surface tension of solutions of electrolytes as a function of the concentration. i. a differential method for measuring relative surface tension. *J Am Chem Soc* 59(1):187–198.
25. Petersen PB, Johnson JC, Knutsen KP, Saykally RJ (2004) Direct experimental validation of the Jones–Ray effect. *Chem Phys Lett* 397(1):46–50.
26. Luo G, et al. (2013) X-ray reflectivity reveals a nonmonotonic ion-density profile perpendicular to the surface of ercl3 aqueous solutions. *J Phys Chem C* 117(37): 19082–19090.
27. Zangi R (2012) Attraction between like-charged monovalent ions. *J Chem Phys* 136(18):184501.
28. Dang LX, Pettitt BM (1990) A theoretical study of like ion pairs in solution. *J Phys Chem* 94(10):4303–4308.
29. Lazaridis T, Paulaitis ME (1992) Entropy of hydrophobic hydration: A new statistical mechanical formulation. *J Phys Chem* 96(9):3847–3855.
30. Benjamin I (1995) Theory and computer simulations of solvation and chemical reactions at liquid interfaces. *Acc Chem Res* 28(5):233–239.
31. Ashbaugh HS, Truskett TM, Debenedetti PG (2002) A simple molecular thermodynamic theory of hydrophobic hydration. *J Chem Phys* 116:2907–2921.
32. Patel HA, Nauman EB, Garde S (2003) Molecular structure and hydrophobic solvation thermodynamics at an octane–water interface. *J Chem Phys* 119(17):9199–9206.
33. Widom B (1963) Some topics in the theory of fluids. *J Chem Phys* 39(11):2808–2812.
34. Hummer G, Pratt LR, García AE (1996) Free energy of ionic hydration. *J Phys Chem* 100(4):1206–1215.
35. Hummer G, Pratt LR, García AE, Berne BJ, Rick SW (1997) Electrostatic potentials and free energies of solvation of polar and charged molecules. *J Phys Chem B* 101(16):3017–3020.
36. Ashbaugh HS (2000) Convergence of molecular and macroscopic continuum descriptions of ion hydration. *J Phys Chem B* 104(31):7235–7238.
37. Rajamani S, Ghosh T, Garde S (2004) Size dependent ion hydration, its asymmetry, and convergence to macroscopic behavior. *J Chem Phys* 120(9):4457–4466.
38. Benjamin L (1993) Mechanism and dynamics of ion transfer across a liquid-liquid interface. *Science* 261(5128):1558–1560.
39. Willard AP, Chandler D (2010) Instantaneous liquid interfaces. *J Phys Chem B* 114(5): 1954–1958.
40. Yang L, Garde S (2007) Modeling the selective partitioning of cations into negatively charged nanopores in water. *J Chem Phys* 126(8):084706.
41. Alejandre J, Tildesley DJ, Chapela GA (1995) Molecular dynamics simulation of the orthobaric densities and surface tension of water. *J Chem Phys* 102(11):4574–4583.
42. Dang LX (1992) Temperature dependence of interactions of an ion pair in water: A molecular dynamics study. *J Chem Phys* 97(3):1919–1921.
43. Zhu S, Elcock AH (2010) A complete thermodynamic characterization of electrostatic and hydrophobic associations in the temperature range 0 to 100 C from explicit-solvent molecular dynamics simulations. *J Chem Theory Comput* 6(4):1293–1306.
44. Weeks JD, Chandler D, Andersen HC (1971) Role of repulsive forces in determining the equilibrium structure of simple liquids. *J Chem Phys* 54(12):5237–5247.
45. Vazquez G, Alvarez E, Navaza J (1995) Surface tension of alcohol + water from 20 to 50 °C. *J Chem Eng Data* 40(3):611–614.
46. Möbius D, Miller R (1998) *Proteins at Liquid Interfaces* (Elsevier, Amsterdam), Vol 7.
47. Hornak V, et al. (2006) Comparison of multiple Amber force fields and development of improved protein backbone parameters. *Proteins* 65(3):712–725.
48. Daura X, et al. (1999) Peptide folding: When simulation meets experiment. *Angew Chem Int Ed* 38(1–2):236–240.
49. Pratt LR, Hummer G, García AE (1994) Ion pair potentials-of-mean-force in water. *Biophys Chem* 51(2–3):147–165.
50. Stamou D, Duschl C, Johannsmann D (2000) Long-range attraction between colloidal spheres at the air-water interface: The consequence of an irregular meniscus. *Phys Rev E Stat Phys Plasmas Fluids Relat Interdiscip Topics* 62(4 Pt B):5263–5272.
51. Nikolaides MG, et al. (2002) Electric-field-induced capillary attraction between like-charged particles at liquid interfaces. *Nature* 420(6913):299–301.
52. de Meyer FJM, Venturoli M, Smit B (2008) Molecular simulations of lipid-mediated protein-protein interactions. *Biophys J* 95(4):1851–1865.
53. Herce HD, Garcia AE (2007) Molecular dynamics simulations suggest a mechanism for translocation of the HIV-1 TAT peptide across lipid membranes. *Proc Natl Acad Sci USA* 104(52):20805–20810.
54. Leunissen ME, Zwanikken J, van Roij R, Chaikin PM, van Blaaderen A (2007) Ion partitioning at the oil-water interface as a source of tunable electrostatic effects in emulsions with colloids. *Phys Chem Chem Phys* 9(48):6405–6414.
55. Loverde SM, Solis FJ, Olvera de la Cruz M (2007) Charged particles on surfaces: Coexistence of dilute phases and periodic structures at interfaces. *Phys Rev Lett* 98(23): 237802.
56. Pronchik J, He X, Giurleo JT, Talaga DS (2010) In vitro formation of amyloid from alpha-synuclein is dominated by reactions at hydrophobic interfaces. *J Am Chem Soc* 132(28):9797–9803.
57. Reddy G, Straub JE, Thirumalai D (2010) Dry amyloid fibril assembly in a yeast prion peptide is mediated by long-lived structures containing water wires. *Proc Natl Acad Sci USA* 107(50):21459–21464.
58. Shenogina N, Godawat R, Keblinski P, Garde S (2009) How wetting and adhesion affect thermal conductance of a range of hydrophobic to hydrophilic aqueous interfaces. *Phys Rev Lett* 102(15):156101.
59. Berendsen HJC, Grigera JR, Straatsma TP (1987) The missing term in effective pair potentials. *J Phys Chem* 91(24):6269–6271.
60. Hess B, Kutzner C, van der Spoel D, Lindahl E (2008) Gromacs 4: Algorithms for highly efficient, load-balanced, and scalable molecular simulation. *J Chem Theory Comput* 4(3):435–447.
61. Hess B, Bekker H, Berendsen HJC, Fraaije JGEM (1997) Lincs: A linear constraint solver for molecular simulations. *J Comput Chem* 18(12):1463–1472.
62. Bussi G, Donadio D, Parrinello M (2007) Canonical sampling through velocity rescaling. *J Chem Phys* 126(1):014101.
63. Darden T, York D, Pedersen L (1993) Particle mesh Ewald - an n.log(n) method for Ewald sums in large systems. *J Chem Phys* 98(12):10089–10092.
64. Hummer G, Szabo A (1996) Calculation of free-energy differences from computer simulations of initial and final states. *J Chem Phys* 105:2004–2010.
65. Kumar S, Bouzida D, Swendsen RH, Kollman PA, Rosenberg JM (1992) The weighted histogram analysis method for free-energy calculations on biomolecules. 1. the method. *J Comput Chem* 13(8):1011–1021.